Accepted manuscript published in *Geochemical Perspective Letters*. doi:10.7185/geochemlet.2109

Preprint doi:10.31223/osf.io/qhtb6

THE COMPOSITION AND WEATHERING OF THE CONTINENTS OVER GEOLOGIC TIME

ACCEPTED, PEER-REVIEWED MANUSCRIPT, COMPILED MARCH 2, 2021

Alex G. Lipp[1*], Oliver Shorttle[2,3], Erik A. Sperling[4], Jochen J. Brocks[5], Devon Cole[6], Peter W. Crockford[7], Lucas Del Mouro[8], Keith Dewing[9], Stephen Q. Dornbos[10], Joseph F. Emmings[11], Una C. Farrell[12], Amber Jarrett[13], Benjamin W. Johnson[14], Pavel Kabanov[9], C. Brehnin Keller[15], Marcus Kunzmann[16], Austin J. Miller[17], N. Tanner Mills[18], Brennan O'Connell[19], Shanan E. Peters[20], Noah J. Planavsky[21], Samantha R. Ritzer[4], Shane D. Schoepfer[22], Philip R. Wilby[11], and Jianghai Yang[23]

[1]Department of Earth Sciences and Engineering, Imperial College London; [2]Department of Earth Sciences, University of Cambridge; [3]Institute of Astronomy, University of Cambridge; [4]Department of Geological Sciences, Stanford University; [5]Research School of Earth Sciences, Australian National University, Canberra; [6]School of Earth and Atmospheric Science, Georgia Institute of Technology; [7]Earth and Planetary Science, Weizmann Institute of Science; [8]Geology Department, Federal University of Santa Catarina; [9]Natural Resources Canada, Geological Survey of Canada, Calgary; [10]Department of Geosciences, University of Wisconsin-Milwaukee; [11]British Geological Survey, Keyworth; [12]Department of Geology, Trinity College Dublin; [13]Onshore Energy Directorate, Geoscience Australia; [14]Department of Geological and Atmospheric Sciences, Iowa State University; [15]Department of Earth Sciences, Dartmouth College; [16]Mineral Resources, CSIRO; [17]Department of Earth and Environmental Sciences, University of Waterloo; [18]Department of Geology and Geophysics, Texas A&M University; [19]School of Earth Sciences, University of Melbourne; [20]Department of Geoscience, University of Wisconsin-Madison; [21]Department of Earth and Planetary Sciences, Yale University; [22]Geoscience and Natural Resources, Western Carolina University; [23]China University of Geosciences, Wuhan

ABSTRACT

The composition of continental crust records the balance between construction by tectonics and destruction by physical and chemical erosion. Quantitative constraints on how igneous addition and chemical weathering have modified the continents' bulk composition are essential for understanding the evolution of geodynamics and climate. Using novel data-analytic techniques we have extracted temporal trends in sediments' protolith composition and weathering intensity from the largest available compilation of sedimentary major-element compositions: ~ 15,000 samples from 4.0 Ga to the present. We find that the average Archean upper continental crust was silica rich and had a similar compositional diversity to modern continents. This is consistent with an early-Archean, or earlier, onset of plate tectonics. In the Archean, chemical weathering sequestered ~ 25 % more CO_2 per mass eroded for the same weathering intensity than in subsequent time periods, consistent with carbon mass-balance despite higher Archean outgassing rates and more limited continental exposure. Since 2.0 Ga, over long (> 0.5 Ga) timescales, crustal weathering intensity has remained relatively constant. On shorter timescales over the Phanerozoic, weathering intensity is correlated to global climate state, consistent with a weathering feedback acting in response to changes in CO_2 sources or sinks.

Keywords Sedimentary Geochemistry · Weathering · Provenance · Archean Continents · Crustal Evolution · Phanerozoic Climate

GRAPHICAL ABSTRACT

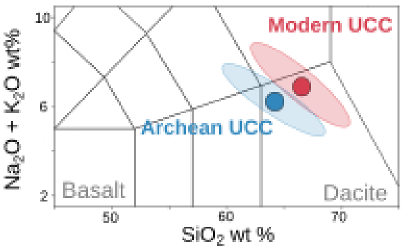

LETTER

Introduction

The rocks at Earth's surface are compositionally divided between dense, silica-poor oceanic crust and a buoyant, silica-rich continental crust. It is generally accepted that this dichotomy is maintained by plate tectonics. The emergence of Earth's first felsic continents therefore could be an indicator for when plate tectonics began. The timing of the earliest felsic continents however remains debated. The Archean (i.e., 2.5 – 4.0 Ga) continents are often viewed as having a mafic composition similar to the oceanic crust (e.g., Taylor and McLennan 1986; Tang et al. 2016) suggesting a late onset for plate tectonics during the Neoarchean, ~ 2.5 Ga. However, a contrasting view has emerged of evolved, silica-rich Archean continents (Greber et al. 2017; Keller and Harrison 2020; Ptáček et al. 2020). This view suggests an earlier onset for plate tectonics before 3.5 Ga.

Not only is the history of the crust necessary for understanding geodynamics, reactions between the crust and hydrosphere stabilise the planet's climate (Broecker and Langmuir 1985). Continental chemical weathering (the alteration of silicate minerals by reaction with water at Earth's surface) transfers atmospheric CO_2 into carbonate minerals deposited on the ocean floor. This reaction is the major long-term sink for CO_2 outgassed by the mantle (Walker et al. 1981; Berner et al. 1983).

The geochemical composition of sedimentary rocks is our primary record of crustal evolution on Gyr timescales. However, this archive is challenging to interpret. Chemical weathering strips sediments of mobile elements altering their composition relative to the rocks from which they derive (protoliths). Signals of changing crustal composition are thus obscured by alteration. Additionally, most sediments record the signals of the local catchment they come from, not the continental crust as a whole. Here, we provide new perspectives into the long-term composition and alteration of the upper continental crust (UCC). We use

***correspondence:** `a.lipp18@imperial.ac.uk`

novel data-analytic methods and the geochemical database produced by the Sedimentary Geochemistry & Paleoenvironments Project.

Methods and Data

Most studies aiming to track changes in crustal composition avoid the alteration of sedimentary compositions by selecting weathering-insensitive elemental ratios. Whilst this approach can resolve protolith changes, by design, it cannot provide information on weathering intensity changes. Here, we simultaneously extract signals of both the weathering intensity of sediments and protolith composition.

To do this we use a new method which explains the major-element (Si, Al, Fe, Mg, Na, Ca, K) composition of sediments in terms of the composition of their protolith, and how intensely they have been weathered (Lipp et al. 2020). This approach constructs a model for a centred log-ratio transformed composition (after Aitchison 1986) $\mathbf{x}'$, as the sum of a weathering vector, $\hat{\mathbf{w}}$, and a protolith vector, $\hat{\mathbf{p}}$, relative to the composition of modern UCC:

$$\mathbf{x}' = \mathbf{UCC} + \omega\hat{\mathbf{w}} + \psi\hat{\mathbf{p}} + \mathbf{E}. \tag{1}$$

The coefficients of these vectors correspond to the weathering intensity experienced by a sediment, ω, and its protolith composition, ψ. Deviations from this model cause the misfit, $\mathbf{E}$, to rise. Sediments with protoliths more(/less) felsic than modern UCC have positive(/negative) ψ values. Weathering of rocks causes ω to rise. Here, we modify this method to correct for the effect of sodium-calcium cation exchange that can occur between dissolved species and those adsorbed to clays (e.g., Sayles and Mangelsdorf 1979). We also use a recalibrated $\hat{\mathbf{w}}$ vector. These modifications reduce the possibility of biases. Some limitations, including diagenesis and marine authigenic clay formation, are discussed in the Supplementary Information but do not significantly affect our results. Please note that the Supplementary Information is found appended to the end of this document.

We apply this method to the compilation of sedimentary geochemical data produced by the Sedimentary Geochemistry & Paleoenvironments (SGP) research consortium (`sgp.stanford.edu`). The SGP database compiles geochemical data and geological context information from three sources: 1) direct data entry by SGP team members (mainly Neoproterozoic-Paleozoic shales with global geographic coverage), 2) the USGS National Geochemical Database (consisting of data from USGS projects from the 1960-1990s; mainly Phanerozoic samples of all lithologies from the United States), and 3) the USGS Critical Metals in Black Shales database (a global shale database spanning all of Earth history). In total we analyse 17,472 major-element compositions each associated with an age. Full details of data, preprocessing and analysis is found in the Supplementary Information.

The Archean protolith

First, we investigate changes in the average composition of the exposed UCC through time. To overcome local heterogeneities we calculate composite samples using the arithmetic mean of all samples in 500 Myr time intervals (Table S1). Because of low sampling density in the Archean, we average all samples older than 2.5 Ga to create an Archean composite. We solve Equation 1 for each composite to calculate ω and ψ, the weathering and protolith coefficients.

Table 1: **Average sediment protolith composition (wt %) through time.** Uncertainties (in the form of a covariance matrix) are given in Table S3

Age, Ga	SiO_2	Al_2O_3	$Fe_2O_3{}^T$	MgO	Na_2O	CaO	K_2O
0 - 0.5	66.5	14.6	5.32	2.32	3.98	4.32	2.95
0.5 - 1.0	67.3	14.5	4.99	2.05	4.04	3.98	3.17
1.0 - 1.5	67.1	14.5	5.06	2.11	4.03	4.05	3.11
1.5 - 2.0	67.3	14.5	5.00	2.06	4.04	3.99	3.16
2.0 - 2.5	66.1	14.7	5.48	2.46	3.95	4.48	2.85
2.5 +	64.1	14.9	6.22	3.16	3.82	5.27	2.46

We can use Equation 1 to reconstruct the full major-element composition of a sediment's protolith from just its ψ value. By substituting the ω value of a sediment in Equation 1 for that of pristine igneous rocks ($\omega_0 = -0.271$; see Supplementary Information) the composition of a sediment's protolith is returned. The calculated compositions of the average sediment protoliths through time are shown in Table 1. These protoliths can be analysed as igneous rocks, with, e.g., a Total Alkali Silica plot (Figure 1). The average Archean protolith was silica-rich and dacitic in composition but slightly more mafic than younger protoliths. This evolved composition for Archean protoliths is similar, albeit marginally more felsic, to the estimate of Ptáček et al. (2020) but arrived at using independent methodologies. The average protolith has remained constant since 2.5 Ga.

As sediments derive from broad regions, their protoliths, in aggregate, can be assumed to be representative of the average exposed crustal composition. Our estimate for the average protolith of recent, < 0.5 Ga, sedimentary rocks (Figure 1) is within error of the estimate of UCC as averaged by surface sampling (Rudnick and Gao 2003), validating this approach. A uniformitarian interpretation of the dacitic Archean UCC is that plate tectonics commenced no later than the early-Archean.

Nonetheless, we note the limitations about inferring global conditions from the small inventory of Archean samples which are highly susceptible to preservation and sampling biases (Korenaga 2013). This low sample-density in the Archean gives low-statistical significance to variability of age-interval means within the Archean (Figure 2a). Evolved igneous rocks could also be generated in the absence of plate tectonics (Reimink et al. 2014).

Focusing exclusively on the average sediment protolith neglects other features in our dataset. The protolith coefficients, ψ, for individual samples through time (Figure 2a) show a large diversity in protoliths throughout Earth's history, including the Archean. If each individual ψ represents a catchment-averaged protolith, then the diversity of rocks at the Earth's surface has remained nearly constant since ~4 Ga. The ψ distributions from before 2.5 Ga are compared to those from 0 - 0.5 Ga in Figure 2b. Whilst the median of the two distributions is different, there is still considerable overlap. The high diversity of exposed rocks, and their on-average evolved nature, suggests that during the Archean the exposed continental crust was more similar to the

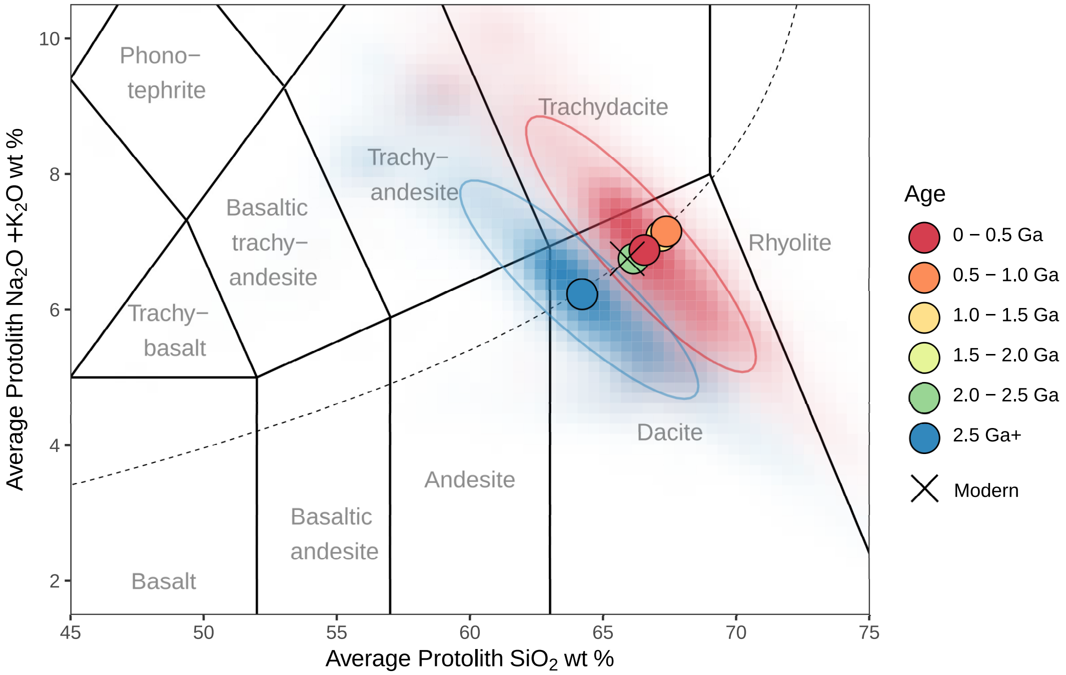

Figure 1: **A dacitic composition for Archean UCC.** Total Alkali-Silica plot displaying the protoliths of the average sediment for different time periods (Le Maitre et al. 2005). Ellipses indicate standard error (see Supplementary Information). '×' is the pristine igneous precursor of the modern upper continental crust (Rudnick and Gao 2003). Dashed line is trend described by $\hat{\mathbf{p}}$.

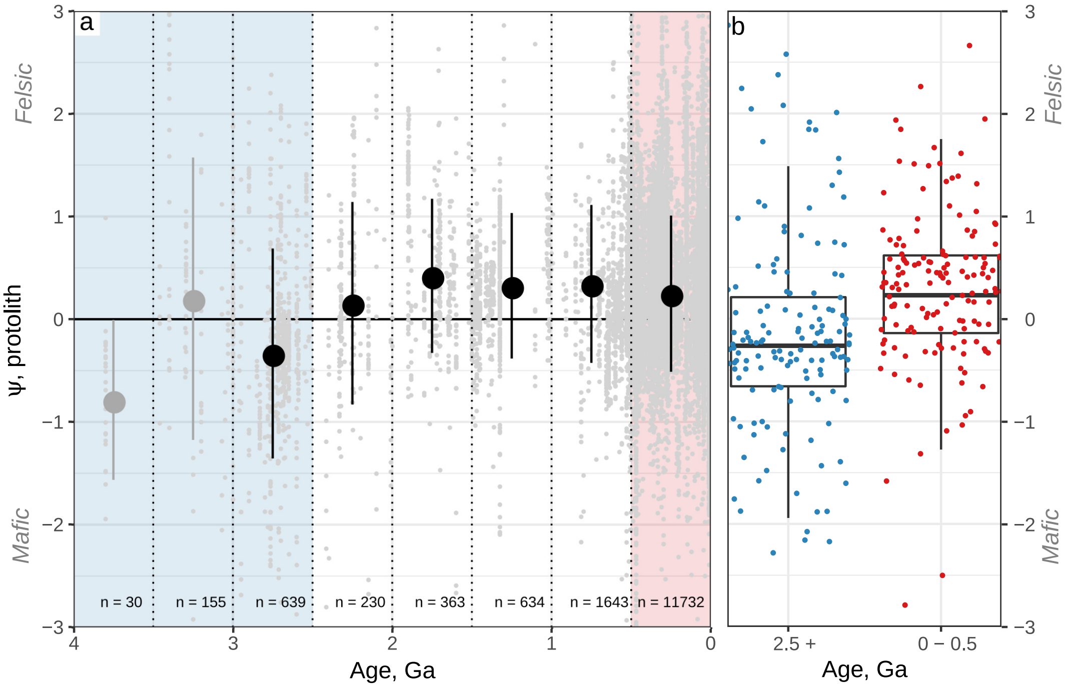

Figure 2: **Archean protoliths were more mafic than the present day but equally diverse.** (a) Grey points are protolith coefficients, ψ, for individual samples. Mean $\psi \pm \sigma$ for each 0.5 Ga time period given by black circles. Means for > 3 Ga greyed out to emphasise low sample coverage. (b) Box-and-whisker comparison of protolith distributions for samples of age > 2.5 and 0 – 0.5 Ga. Whiskers extend 1.5 × interquartile-range from the upper/lower-quartiles. 200 randomly selected samples shown for each age group.

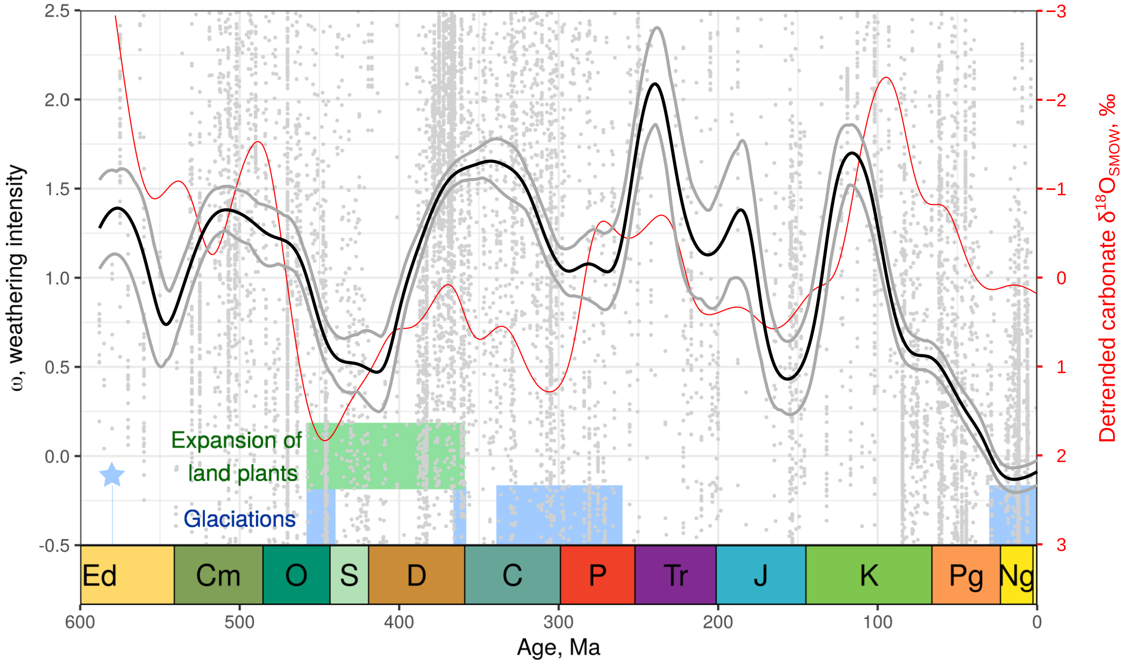

Figure 3: **Weathering intensity of sedimentary rocks across the Phanerozoic.** Grey points are individual samples, black line is smoothed trend calculated using 30 Myr bandwidth Gaussian kernel, and grey lines show bootstrap uncertainty (see Supplementary Information). Red line is detrended Oxygen isotope composition of carbonates smoothed using 30 Myr bandwidth Gaussian. Data from δ^{18}O compilation of Jaffrés et al. (2007). Periods of glaciation (star for emphasis) and land-plant expansion from Pu et al. (2016), McMahon and Davies (2018), and Macdonald et al. (2019)

modern crust than it was different. Near-constant protolith diversity from the Archean to Recent is independently evidenced by the ratio of felsic to mafic igneous rocks in a comprehensive compilation of geologic columns in North America (Figure S5; Peters et al. 2018). This near-constant protolith diversity supports uniformitarian models of petrogenetic processes, e.g., long lived plate-tectonics.

Crustal weathering on billion year timescales

Second, we explore how the efficiency of CO_2 drawdown by crustal weathering may have evolved through time. The weathering of mafic rocks sequesters more CO_2 than felsic rocks due to their higher concentrations of Ca and Mg (e.g., Dessert et al. 2003). The more mafic Archean UCC could result in more CO_2 sequestered per mass of rock weathered than modern UCC. This effect could potentially bring the weathering CO_2 sink in balance with mantle outgassing despite a smaller exposed continental area (Albarede et al. 2020). To quantify this effect, we calculate the chemical depletion fraction for any $\omega - \psi$ pair, assuming that Al_2O_3 is immobile (Brimhall and Dietrich 1987; see Supplementary Information). The mass of each element mobilised due to weathering per kg of protolith eroded can then be converted into moles of carbonate-bound CO_2 assuming the stoichiometry

$$CaSiO_3 + CO_2 \longrightarrow CaCO_3 + SiO_2,$$

and efficient Mg-Ca exchange at mid-ocean ridges (Holland 1984). Any $\omega - \psi$ pair can thus be converted into a (maximum) amount of CO_2 deposited per kg of weathered protolith (Figure S2a).

Weathering the Archean protolith sequesters ~ 25 % more CO_2 than subsequent protoliths for the same weathering intensity (Figure S2b). Since the Archean, the CO_2 sequestered per kg UCC eroded has not changed considerably (Figure S2a). On timescales greater than 0.5 Gyr therefore, any change in Earth's total weathering flux must have been achieved by changing the absolute amount of erosion, not the weathering intensity. Hence, to maintain an equitable climate over these timescales, secular changes in volcanic CO_2 outgassing must have been compensated for by changes in amounts of physical erosion. Alternatively, changes to other aspects of the carbon-cycle could have taken place (e.g., changing the reverse-weathering flux; Isson and Planavsky 2018).

Crustal weathering over the Phanerozoic

Finally, we explore how global weathering intensity has changed during the Phanerozoic. On 10 – 100 Myr timescales, weathering intensity is believed to respond to global climate state as part of a negative feedback (Walker et al. 1981; Berner et al. 1983). Individual sediments only record the weathering intensity of their source regions, but collectively they may reflect these global shifts in silicate weathering intensity.

Figure 3 shows the weathering coefficient, ω, for the ~ 12,000 samples less than 600 Ma. The lowest weathering intensity occurs in the Neogene. Other periods of low intensity are observed in the late Ordovician/Silurian, late Permian and the Jurassic. Peaks in weathering intensity are found in the Carboniferous, Triassic and Cretaceous. We find that sampling biases do not strongly affect these observations (see Supplementary Information; Figure S4).

The ω fluctuations we observe are on timescales too long (10's Myr) to be explained by the silicate weathering feedback acting in response to short-term climatic perturbations. The weathering intensity trend is instead consistent with long-term CO_2 mass-balance forced by changes in the magnitude of carbon sources and sinks. For example, an increased flux of volcanic CO_2 would result initially in an imbalance in the geologic carbon cycle, as the weathering sink is unchanged. However, as atmospheric CO_2 rises on Myr timescales, the weathering intensity of rocks should rise due to higher pCO2 driving warmer and wetter conditions. The carbon cycle will then achieve balance albeit at an elevated CO_2 level and altered climate state. An increase in carbon sinks driven by, e.g., mountain building, would have the opposite effect. The global intensity of weathering hence changes in concert with the balance of carbon sources and sinks (e.g., Raymo and Ruddiman 1992; Berner and Caldeira 1997; McKenzie et al. 2016).

This hypothesis predicts a positive correlation between the average surface temperature and weathering intensity. We can test these predictions by comparing the smoothed weathering trend to climate proxies. First we consider the detrended oxygen isotope composition of marine carbonates, considered a proxy for global climate (Veizer et al. 2000). When the $\delta^{18}O$ of marine carbonates is heavy (associated with cooler climates) we observe a lower weathering intensity while the opposite is true for lighter $\delta^{18}O$ (associated with warmer climates).

The validity of the $\delta^{18}O$ record however is controversial as it is susceptible to diagenetic overprinting (e.g., Ryb and Eiler 2018). As a result we also compare our ω record to a more unambiguous record of climate state: evidence of glaciated poles. We observe local minima in chemical weathering intensity during ice-house climates (Ordovician-Silurian, Permian, Neogene). We note however that the end-Devonian glaciation coincides with a period of observed high weathering intensity. These observations generally match the relationship between weathering intensities and climate state that is predicted by carbon mass-balance.

The lack of a state-change in weathering intensity following the Paleozoic emergence of land-plants further illustrates the importance of carbon mass balance. The expansion of land-plants, by increased pedogenesis, initially caused an increase in the weathering carbon sink. The resulting carbon-cycle imbalance is then resolved by a decrease in weathering intensity by the mechanism described above (e.g., Algeo et al. 1995). Hence, only a transient ω response is observed in response to the step-wise expansion of land-plants.

Summary

A large inventory of sedimentary rock major-element compositions has been deconvolved into a record of crustal composition and weathering intensity. Results indicate an evolved and heterogeneous Archean crust, which suggests an early onset of plate tectonics. Weathering of this Archean crust was ~ 25 % more efficient at sequestering atmospheric CO_2 than modern day UCC. On long, Gyr, timescales the weathering intensity of the crust has remained constant. By contrast, on short, 100 Myr, timescales weathering intensity responds to global climate shifts consistent with a silicate weathering feedback responding to changes in carbon sources or sinks.

Data and Code Availability

An annotated R-markdown notebook which performs all the calculations described below in R and python can be found at `github.com/AlexLipp/crustal-comp` (Van Rossum and Drake 2009; R Core Team 2018). The data used for our reported results and the SQL command used to query the SGP database are also found at the same location. Scripts and data are archived at the point of submission at `doi.org/10.5281/zenodo.4309952`.

Acknowledgements

AGL is funded by the Natural Environment Research Council Grantham Institute SSCP DTP (grant number NE/L002515/1). OS acknowledges support from NERC grants NE/T012455/1 & NE/T00696X/1. This work was supported by CASP. British Geological Survey authors (JFE, PRW) publish with permission of the Executive Director of the British Geological Survey, UKRI. We thank Gareth Roberts for helpful comments. The authors are grateful to Julie Dumoulin, Clinton Scott, Akshay Mehra, Justin Strauss, Jon Husson, Tristan White, Tiffani Fraser (Yukon Geological Survey), Ben Gill, Florian Kurzweil, Danielle Thomson, Wing Chan, Joseph Magnall and Lawrence Och for their contributions to the Sedimentary Geochemistry and Paleoenvironments Project.

Author Contributions

AGL and OS conceived of the study. AGL performed data analysis and prepared the manuscript. EAS led development of the Sedimentary Geochemistry and Paleoenvironments Project. JJB, DC, PWC, LDM, KD, SQD, JFE, UCF, AJ, BWJ, PK, CBK, MK, AJM, NTM, BOC, SEP, NJP, SRR, SDS, PRW and JY all contributed to the Sedimentary Geochemistry and Paleoenvironments Project. JFE helped guide discussion of the role of diagenesis. NJP helped guide discussion of Phanerozoic carbon cycle. SEP produced Figure S5. All authors contributed to manuscript revision.

References

Aitchison, J. (1986). *The statistical analysis of compositional data*. Chapman and Hall.

Albarede, F., F. Thibon, J. Blichert-Toft, and H. Tsikos (2020). "Chemical archeoceanography". *Chemical Geology* 548, p. 119625. doi: `10.1016/j.chemgeo.2020.119625`.

Algeo, T. J., R. A. Berner, J. B. Maynard, and S. E. Scheckler (1995). "Late Devonian Oceanic Anoxic Events and Biotic Crises: "Rooted" in the Evolution of Vascular Land Plants?" *GSA TODAY*, p. 24.

Berner, R. A. and K. Caldeira (1997). "The need for mass balance and feedback in the geochemical carbon cycle". *Geology* 25.10, pp. 955–956. doi: `10.1130/0091-7613(1997)025<0955:TNFMBA>2.3.CO;2`.

Berner, R. A., A. C. Lasaga, and R. M. Garrels (1983). "The carbonate-silicate geochemical cycle and its effect on atmospheric carbon dioxide over the past 100 million years". *American Journal of Science* 283.7, pp. 641–683. doi: `10.2475/ajs.283.7.641`.

Bjørlykke, K. and J. Jahren (2012). "Open or closed geochemical systems during diagenesis in sedimentary basins: Constraints on mass transfer during diagenesis and the prediction of porosity in sandstone and carbonate reservoirs". *AAPG Bulletin* 96.12, pp. 2193–2214. doi: 10.1306/04301211139.

Brimhall, G. H. and W. E. Dietrich (1987). "Constitutive mass balance relations between chemical composition, volume, density, porosity, and strain in metasomatic hydrochemical systems: Results on weathering and pedogenesis". *Geochimica et Cosmochimica Acta* 51.3, pp. 567–587. doi: 10.1016/0016-7037(87)90070-6.

Broecker, W. S. and C. H. Langmuir (1985). "Making it comfortable". In: *How to build a habitable planet*. Princeton University Press, pp. 298–386.

Cerling, T. E., B. L. Pederson, and K. L. V. Damm (1989). "Sodium-calcium ion exchange in the weathering of shales: Implications for global weathering budgets". *Geology* 17.6, pp. 552–554. doi: 10.1130/0091-7613(1989)017<0552:SCIEIT>2.3.CO;2.

Dessert, C., B. Dupré, J. Gaillardet, L. M. François, and C. J. Allègre (2003). "Basalt weathering laws and the impact of basalt weathering on the global carbon cycle". *Chemical Geology*. Controls on Chemical Weathering 202.3, pp. 257–273. doi: 10.1016/j.chemgeo.2002.10.001.

Devaraju, T. C., T. L. Sudhakara, R. J. Kaukonen, R. P. Viljoen, T. T. Alapieti, S. A. Ahmed, and S. Sivakumar (2010). "Petrology and geochemistry of greywackes from Goa-Dharwar sector, western Dharwar Craton: Implications for volcanoclastic origin". *Journal of the Geological Society of India* 75.3, pp. 465–487. doi: 10.1007/s12594-010-0050-8.

Fedo, C. M., K. A. Eriksson, and E. J. Krogstad (1996). "Geochemistry of shales from the Archean (~3.0 Ga) Buhwa Greenstone Belt, Zimbabwe: Implications for provenance and source-area weathering". *Geochimica et Cosmochimica Acta* 60.10, pp. 1751–1763. doi: 10.1016/0016-7037(96)00058-0.

Greber, N. D., N. Dauphas, A. Bekker, M. P. Ptáček, I. N. Bindeman, and A. Hofmann (2017). "Titanium isotopic evidence for felsic crust and plate tectonics 3.5 billion years ago". *Science* 357.6357, pp. 1271–1274. doi: 10.1126/science.aan8086.

Holland, H. D. (1984). *The Chemical Evolution of the Atmosphere and Oceans*. Princeton University Press. 600 pp.

Isson, T. T. and N. J. Planavsky (2018). "Reverse weathering as a long-term stabilizer of marine pH and planetary climate". *Nature* 560.7719, pp. 471–475. doi: 10.1038/s41586-018-0408-4.

Jaffrés, J. B. D., G. A. Shields, and K. Wallmann (2007). "The oxygen isotope evolution of seawater: A critical review of a long-standing controversy and an improved geological water cycle model for the past 3.4 billion years". *Earth-Science Reviews* 83.1, pp. 83–122. doi: 10.1016/j.earscirev.2007.04.002.

Jiang, H. and C.-T. A. Lee (2019). "On the role of chemical weathering of continental arcs in long-term climate regulation: A case study of the Peninsular Ranges batholith, California (USA)". *Earth and Planetary Science Letters* 525, p. 115733. doi: 10.1016/j.epsl.2019.115733.

Keller, C. B. and T. M. Harrison (2020). "Constraining crustal silica on ancient Earth". *Proceedings of the National Academy of Sciences*. doi: 10.1073/pnas.2009431117.

Korenaga, J. (2013). "Initiation and Evolution of Plate Tectonics on Earth: Theories and Observations". *Annual Review of Earth and Planetary Sciences* 41.1, pp. 117–151. doi: 10.1146/annurev-earth-050212-124208.

Le Maitre, R. W., A. Streckeisen, B. Zanettin, M. J. Le Bas, B. Bonin, and P. Bateman (2005). *Igneous Rocks: A Classification and Glossary of Terms*. Cambridge University Press. 252 pp.

Lipp, A. G., O. Shorttle, F. Syvret, and G. G. Roberts (2020). "Major Element Composition of Sediments in Terms of Weathering and Provenance: Implications for Crustal Recycling". *Geochemistry, Geophysics, Geosystems* 21.6, e2019GC008758. doi: 10.1029/2019GC008758.

Lupker, M., C. France-Lanord, and B. Lartiges (2016). "Impact of sediment–seawater cation exchange on Himalayan chemical weathering fluxes". *Earth Surface Dynamics* 4.3, pp. 675–684. doi: https://doi.org/10.5194/esurf-4-675-2016.

Macdonald, F. A., N. L. Swanson-Hysell, Y. Park, L. Lisiecki, and O. Jagoutz (2019). "Arc-continent collisions in the tropics set Earth's climate state". *Science* 364.6436, pp. 181–184. doi: 10.1126/science.aav5300.

McKenzie, N. R., B. K. Horton, S. E. Loomis, D. F. Stockli, N. J. Planavsky, and C.-T. A. Lee (2016). "Continental arc volcanism as the principal driver of icehouse-greenhouse variability". *Science* 352.6284, pp. 444–447. doi: 10.1126/science.aad5787.

McMahon, W. J. and N. S. Davies (2018). "Evolution of alluvial mudrock forced by early land plants". *Science* 359.6379, pp. 1022–1024. doi: 10.1126/science.aan4660.

Nesbitt, H. W., G. M. Young, and S. A. Bosman (2009). "Major and trace element geochemistry and genesis of supracrustal rocks of the North Spirit Lake Greenstone belt, NW Ontario, Canada". *Precambrian Research* 174.1, pp. 16–34. doi: 10.1016/j.precamres.2009.06.006.

Peters, S. E., J. M. Husson, and J. Czaplewski (2018). "Macrostrat: A Platform for Geological Data Integration and Deep-Time Earth Crust Research". *Geochemistry, Geophysics, Geosystems* 19.4, pp. 1393–1409. doi: https://doi.org/10.1029/2018GC007467.

Ptáček, M. P., N. Dauphas, and N. D. Greber (2020). "Chemical evolution of the continental crust from a data-driven inversion of terrigenous sediment compositions". *Earth and Planetary Science Letters* 539, p. 116090. doi: 10.1016/j.epsl.2020.116090.

Pu, J. P., S. A. Bowring, J. Ramezani, P. Myrow, T. D. Raub, E. Landing, A. Mills, E. Hodgin, and F. A. Macdonald (2016). "Dodging snowballs: Geochronology of the Gaskiers glaciation and the first appearance of the Ediacaran biota". *Geology* 44.11, pp. 955–958. doi: 10.1130/G38284.1.

R Core Team (2018). *R: A Language and Environment for Statistical Computing*. Vienna, Austria.

Raymo, M. E. and W. F. Ruddiman (1992). "Tectonic forcing of late Cenozoic climate". *Nature* 359.6391, pp. 117–122. doi: 10.1038/359117a0.

Reimink, J. R., T. Chacko, R. A. Stern, and L. M. Heaman (2014). "Earth's earliest evolved crust generated in an Iceland-like setting". *Nature Geoscience* 7.7, pp. 529–533. doi: 10.1038/ngeo2170.

Rudnick, R. L. and S. Gao (2003). "Composition of the Continental Crust". *Treatise on Geochemistry* 3, p. 659. DOI: `10.1016/B0-08-043751-6/03016-4`.

Ryb, U. and J. M. Eiler (2018). "Oxygen isotope composition of the Phanerozoic ocean and a possible solution to the dolomite problem". *Proceedings of the National Academy of Sciences* 115.26, pp. 6602–6607. DOI: `10.1073/pnas.1719681115`.

Sayles, F. L. and P. C. Mangelsdorf (1979). "Cation-exchange characteristics of Amazon River suspended sediment and its reaction with seawater". *Geochimica et Cosmochimica Acta* 43.5, pp. 767–779. DOI: `10.1016/0016-7037(79)90260-6`.

Sepkoski, J. J. (1993). "Ten Years in the Library: New Data Confirm Paleontological Patterns". *Paleobiology* 19.1, pp. 43–51.

Sun, X., J. Higgins, and A. V. Turchyn (2016). "Diffusive cation fluxes in deep-sea sediments and insight into the global geochemical cycles of calcium, magnesium, sodium and potassium". *Marine Geology* 373, pp. 64–77. DOI: `10.1016/j.margeo.2015.12.011`.

Tang, M., K. Chen, and R. L. Rudnick (2016). "Archean upper crust transition from mafic to felsic marks the onset of plate tectonics". *Science* 351.6271, pp. 372–375. DOI: `10.1126/science.aad5513`.

Taylor, S. R. and S. M. McLennan (1986). "The chemical composition of the Archaean crust". *Geological Society, London, Special Publications* 24.1, pp. 173–178. DOI: `10.1144/GSL.SP.1986.024.01.16`.

Torres, M. A., A. J. West, and G. Li (2014). "Sulphide oxidation and carbonate dissolution as a source of CO2 over geological timescales". *Nature* 507.7492, pp. 346–349. DOI: `10.1038/nature13030`.

Van Rossum, G. and F. L. Drake (2009). *Python 3 Reference Manual*. Scotts Valley, CA: CreateSpace.

Veizer, J., Y. Godderis, and L. M. François (2000). "Evidence for decoupling of atmospheric CO 2 and global climate during the Phanerozoic eon". *Nature* 408.6813, pp. 698–701. DOI: `10.1038/35047044`.

Walker, J. C. G., P. B. Hays, and J. F. Kasting (1981). "A negative feedback mechanism for the long-term stabilization of Earth's surface temperature". *Journal of Geophysical Research: Oceans* 86 (C10), pp. 9776–9782. DOI: `10.1029/JC086iC10p09776`.

Wallmann, K., G. Aloisi, M. Haeckel, P. Tishchenko, G. Pavlova, J. Greinert, S. Kutterolf, and A. Eisenhauer (2008). "Silicate weathering in anoxic marine sediments". *Geochimica et Cosmochimica Acta* 72.12, pp. 2895–2918. DOI: `10.1016/j.gca.2008.03.026`.

White, A. F., T. D. Bullen, M. S. Schulz, A. E. Blum, T. G. Huntington, and N. E. Peters (2001). "Differential rates of feldspar weathering in granitic regoliths". *Geochimica et Cosmochimica Acta* 65.6, pp. 847–869. DOI: `10.1016/S0016-7037(00)00577-9`.

Young, K. E., C. A. Evans, K. V. Hodges, J. E. Bleacher, and T. G. Graff (2016). "A review of the handheld X-ray fluorescence spectrometer as a tool for field geologic investigations on Earth and in planetary surface exploration". *Applied Geochemistry* 72, pp. 77–87. DOI: `10.1016/j.apgeochem.2016.07.003`.

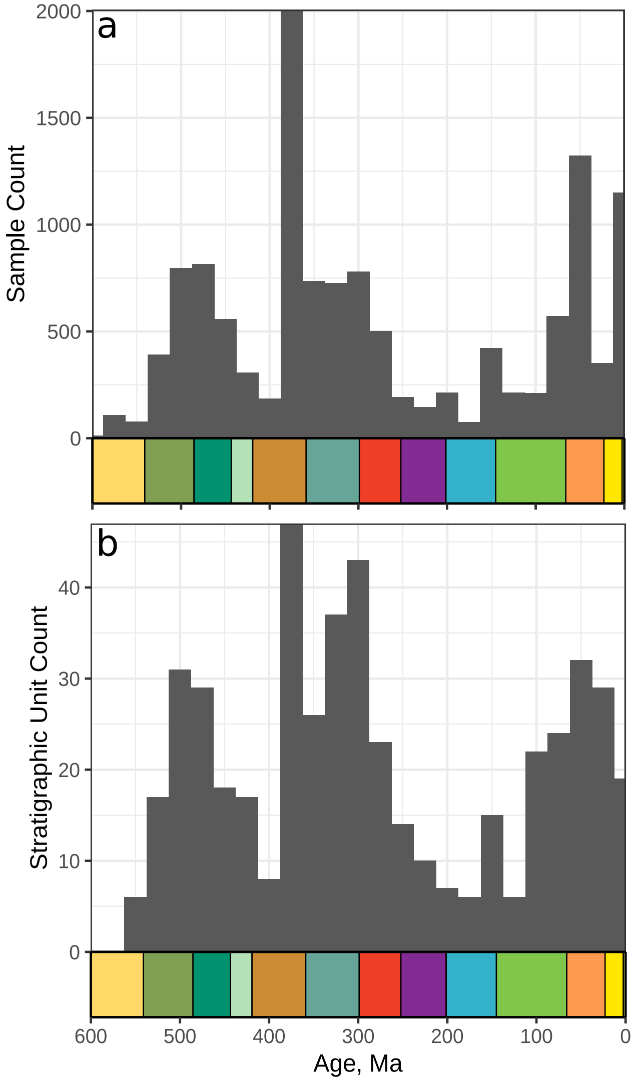

Supplementary Figure 1: **Temporal sampling density of dataset** (a) Histogram of ages for all samples included in dataset with binwidth equal to 25 Myr. Coloured boxes indicate geological periods (see Figure 3). (b) Same as panel a but for the number of individual stratigraphic units sampled, as defined by the SGP dataset.

SUPPLEMENTARY INFORMATION

Data

The Sedimentary Geochemistry and Paleoenvironments Project (SGP) is a research consortium that has produced the largest available compilation of sedimentary geochemical data from across Earth's history. This compilation is being analysed for a range of different research questions, in addition to this study. The project combines pre-existing large datasets, such as the United States Geological Survey (USGS) National Geochemical Database and Critical Metals in Black Shales compilations, with new data gathered from temporal gaps identified in the record. Each sample in the dataset is accompanied with contextual data relating to their stratigraphic and geographic position, including an interpreted absolute age. More information can be found at the project's homepage at `sgp.stanford.edu/about`. The current phase of SGP focuses primarily on the Phanerozoic and so for the Precambrian aspects of this study it was supplemented with the compilation from Lipp et al. (2020) and further literature data (Fedo et al. 1996; Nesbitt et al. 2009; Devaraju et al. 2010). A histogram of how these samples are distributed in time is given in Figure S1.

Supplementary Table 1: **Composite sediment compositions through time.**

Age, Ga	SiO_2	Al_2O_3	$Fe_2O_3{}^T$	MgO	Na_2O	CaO	K_2O
0 - 0.5	71.7	13.7	5.12	2.35	1.14	2.99	3.06
0.5 - 1.0	70.0	15.6	5.42	2.18	1.26	1.79	3.77
1.0 - 1.5	68.4	16.4	5.97	2.34	1.32	1.53	4.08
1.5 - 2.0	66.6	17.1	6.00	2.51	1.09	2,13	4.58
2.0 - 2.5	66.0	17.6	7.46	2.41	1.86	1.25	3.46
2.5 +	65.1	17.0	7.70	3.29	2.08	1.84	3.00

From this database, we query for samples which contain measurements of all the seven elements required for our method (Si, Al, Mg, Fe, Na, Ca, K), by any analytical method except for Handheld X-Ray Fluorescence (HHXRF). HHXRF is excluded as it is sensitive to sample preparation which cannot easily be controlled for potentially introducing artefacts. Additionally, HHXRF cannot reliably produce data for Mg and Na, both of which are required for our data analysis (Young et al. 2016). In any large data compilation, there are concerns about underlying data quality. Because our analyses require Si, and we have excluded Handheld XRF data, most data will have been generated using benchtop XRF instruments. The higher abundance of XRF data is because ICP methodologies frequently do not produce Si data, although this depends on the sample dissolution protocol used. As most data is generate by one methodology, possible biases between analyses are reduced. Additionally, individual measurement errors will not affect overall patterns in large datasets as long as there are not systematic biases in the dataset (e.g., Sepkoski 1993). It is thus unlikely there are errors resulting from original analyses that are driving our results. Further, almost all data are from the published literature or accredited laboratories (e.g., USGS data) and therefore meet these levels of independent community approval. Thus, geochemical measurement errors are unlikely to affect our results.

The data presented here is compiled from hundreds of sources, mostly from published academic literature. Whilst precautions have been applied to ensure a high-quality of data, and much of the data has already been scrutinised under peer-review, it has not been independently verified in this study. The data presented should be treated with the same scrutiny applied to any published data.

After obtaining these data, the elemental compositions are converted into wt% oxides, with total iron given as Fe_2O_3. The results of our method are the same whether or not the composition is normalised to 100 % prior to analysis.

Data Screening

To ensure the reliability of our input data, we screen certain samples from the data extracted from the SGP database. First, we remove any manually identified duplicates which are present due to overlap between the literature compililation of Lipp et

Supplementary Table 2: **Centred log-ratio transformed vectors used to solve Equation 1**

	SiO_2	Al_2O_3	$Fe_2O_3{}^T$	MgO	Na_2O	CaO	K_2O
UCC	2.33	0.869	-0.142	-0.957	-0.681	-0.587	-0.836
$\hat{\mathbf{w}}$	0.242	0.369	0.235	0.133	-0.487	-0.678	0.186
$\hat{\mathbf{p}}$	0.234	0.098	-0.231	-0.601	0.248	-0.336	0.589

al. (2020) and any literature data within the SGP dataset. Second, we exclude any samples for which the lithology is not listed as siliciclastic. Finally, from these siliciclastic sediments we exclude samples which are likely to have been affected by carbonate contamination. How these carbonate contaminated samples are identified is described in further detail below.

Composite Samples

Composite sediment samples are generated by mixing (i.e, taking the arithmetic mean) of all samples within 500 Ma intervals. Due to low sample density in the Archean, all samples older than 2.5 Ga were mixed to generate an Archean composite. If composite samples are created in 500 Ma bins in the Archean, there are some minor changes to the results. The 3.5 - 4.0 Ga interval produces an Andesitic protolith, and the 3.0 - 3.5 Ga has a protolith similar to that from the time period 0 - 0.5 Ga. However, given the low sampling density (the 3.5 - 4.0 Ga interval contains only 30 samples all from the Isua Greenstone Belt), this temporal variance is likely strongly affected by local variability. There is no reasonable binning procedure which results in a protolith of any time-interval more mafic than an Andesite.

Data Analytical Methods

The method we use was developed and detailed in full in Lipp et al. (2020). This method deconvolves the major-element composition of a sediment into the contribution due to changes in protolith and changes caused by chemical weathering. This method has a number of benefits relative to previous compositional analytical approaches such as: insensitivity to the issues of the ‘closure effect’, the ability to reconstruct the full composition of protoliths, and a quantitative measure of misfit.

This approach works by constructing a 2D vector addition model to explain the major-element compositions of sediments. This model is shown in Equation 1 in the main manuscript and repeated here:

$$\mathbf{x}' = \mathbf{UCC} + \omega\hat{\mathbf{w}} + \psi\hat{\mathbf{p}} + \mathbf{E}.$$

This model is only applied to a composition, $\mathbf{x}$, after they have undergone a centred log-ratio, *clr*, transformation to resolve the ‘closure’ effect inherent to compositional data (Aitchison 1986). Hence, $clr(\mathbf{x}) = \mathbf{x}'$. The unit vectors corresponding to weathering and protolith, $\hat{\mathbf{w}}$ and $\hat{\mathbf{p}}$ respectively, were calibrated on independent data. $\hat{\mathbf{w}}$ was calibrated using a soil profile, and $\hat{\mathbf{p}}$ was calibrated using a suite of cogenetic igneous rocks. The model calibrated in this way was successful in extracting information of weathering intensity and protolith from sedimentary compositions and explained the majority of the observed variance. However, residual analysis indicated two potential points at which the model could be improved.

First, $\hat{\mathbf{w}}$ was noted to be slightly miscalibrated, causing a systematic increase in misfit with increasing weathering intensity. This miscalibration was likely caused by calibrating $\hat{\mathbf{w}}$ on a single profile, which will incorporate localised noise. For this study, to derive a better calibrated vector we take a ‘consensus’ $\hat{\mathbf{w}}$ of two different profiles. Specifically it is the arithmetic mean of the first principal components of the soil profile reported in White et al. (2001) and the ‘Toorongo’ soil profile that was used individually to calibrate the original $\hat{\mathbf{w}}$. This better calibrated $\hat{\mathbf{w}}$ ameliorates the issue of rising misfit with greater weathering intensity. All the vectors utilised in Equation 1 are given in Table S2.

Secondly, a relationship between *clr*(Ca) and *clr*(Na) residuals was noted. This relationship was interpreted to be related to cation exchange of Ca and Na which is increasingly recognised as playing a significant impact on geochemical cycles (Sayles and Mangelsdorf 1979; Cerling et al. 1989; Lupker et al. 2016). Subsequently it was observed that cation exchange could cause, minor, spurious changes in ω and ψ if it was not explicitly taken into account. As a result, in this study we include a cation exchange correction into our model. Hence, our model is now:

$$\mathbf{x}' = \mathbf{UCC} + \omega\hat{\mathbf{w}} + \psi\hat{\mathbf{p}} + f(\chi) + \mathbf{E}.$$

This correction factor simply shifts compositions which have been offset from model plane due to cation exchange, back onto the 2D plane indicated in Equation 1. In this formulation $f(\chi)$ varies the proportion of total Ca and Na which taken up by Ca, χ, according to the stoichiometry:

$$\mathrm{Na}_{2,\mathrm{clay}} + \mathrm{Ca}^{2+} \rightleftharpoons 2\,\mathrm{Na}^{+} + \mathrm{Ca}_{\mathrm{clay}}\,.$$

χ therefore ranges between 0 and 1. $f(\chi)$ is non-linear so this equation has no analytical solutions. To find ω, ψ and χ we therefore numerically minimise $|\mathbf{E}|$ using a gradient descent algorithm implemented in `python`.

When increasing the components of any model there is always a tradeoff between over- and under-fitting data. We choose to explicitly consider cation exchange as a process as not doing so introduced some minor biases into our results. Nonetheless, this increases the risk that other processes not explicitly included in the model act to alias the results. We found that the major results of this study were invariant to including cation exchange or not.

Calculating Protolith Compositions

Consider a *clr* transformed major-element composition $\mathbf{x}'$. We solve Equation 1 to calculate its ω and ψ values. These coefficients can be interpreted in terms of translating a protolith composition parallel to the weathering vector a distance equal to ‘ω’. This translation is performed relative to a protolith composition equal to $\mathbf{UCC} + \psi\hat{\mathbf{p}}$. Hence, to calculate the protolith composition we simply translate back along the weathering vector to the original ω value. As a result, we need to calculate an ω value which corresponds to pristine igneous rocks, i.e., ω_0. Previously this was done by calculating the mean ω value of a large suite of igneous rocks taken from the NAVDAT (`www.navdat.org`) database (see Lipp et al. 2020). Performing this calculation on the same compilation of igneous rocks for our updated $\hat{\mathbf{w}}$ vector gives an $\omega_0 = -0.271$.

	$c(SiO_2)$	$c(Al_2O_3)$	$c(Fe_2O_3)$	$c(MgO)$	$c(Na_2O)$	$c(CaO)$	$c(K_2O)$
$c(SiO_2)$	0.071	0.047	-0.050	-0.014	0.008	0.006	-0.068
$c(Al_2O_3))$	0.047	0.066	-0.039	-0.025	0.010	0.008	-0.068
$c(Fe_2O_3)$	-0.050	-0.039	0.132	-0.058	0.000	0.000	0.016
$c(MgO)$	-0.014	-0.025	-0.058	-0.062	-0.008	-0.007	0.050
$c(Na_2O)$	0.008	0.010	0.000	-0.008	0.003	0.001	-0.014
$c(CaO)$	0.006	0.008	0.000	-0.007	0.001	0.002	-0.010
$c(K_2O)$	-0.068	-0.068	0.016	0.050	-0.014	-0.010	0.094

Supplementary Table 3: **Covariance matrix for reconstructed protoliths shown in Table 1** Note that this is for *clr* variables. This matrix is the closest multivariate analogy to a standard deviation.

Quantifying Uncertainties

Projecting all igneous variability onto a single 1D vector, $\hat{\mathbf{p}}$, is obviously a simplification, albeit a useful one. When we calculate protolith compositions as described above, any variability excluded from this 1D vector is neglected. A useful measure of uncertainity in the protolith calculations therefore is how much natural variability there is of real igneous rocks relative to this $\hat{\mathbf{p}}$ trend. To calculate this variability we solve Equation 1 for the NAVDAT compilation of igneous rocks described above. The variability of igneous rocks around the trend, is hence the misfit matrix $\mathbf{E}$ for the NAVDAT dataset. If a multivariate gaussian uncertainity distribution is assumed we can therefore define $cov(\mathbf{E}_{NAVDAT})$. This covariance matrix is the closest multivariate analogy to a standard deviation for our estimates of protolith composition. $cov(\mathbf{E}_{NAVDAT})$ is given in Table 3.

To generate the uncertainty distributions shown in Figure 1 we simply add this derived $\mathbf{E_{NAVDAT}}$ matrix to the calculated *clr* protolith compositions, and then perform the inverse *clr* transformation. To turn this empirical distribution on the TAS plot into a confidence ellipse on Figure 1 we fit a 2D t-student distribution and demarcate the standard error of the mean ellipse, i.e., the 68.3 % interval.

Quantifying CO_2 drawdown

If a sediment's protolith composition is known, the relative loss of a specific element due to weathering can be calculated using the chemical depletion fraction, assuming an immobile element (e.g., Jiang and Lee 2019). In this study we calculate the sediment protolith composition, $\mathbf{x_0}$, from an observed composition, $\mathbf{x_1}$, using the method described above and use aluminium as an immobile element. Hence

$$f_i = \frac{\Delta M_i}{M_{i,0}} = \frac{x_{i,1}}{x_{i,0}} \cdot \frac{x_{Al_2O_3,0}}{x_{Al_2O_3,1}} - 1.$$

In this formulation, $\mathbf{f}$ is the kg of each component lost due to weathering for each kg of initial protolith, $M_{i,0}$ is the initial mass of the i^{th} component of a composition and ΔM_i is the change in mass of that same component due to weathering. Using this formula and Equation 1 it is possible to calculate the relative loss of each element due to weathering for a given $\omega - \psi$ pair. Converting from the mass of CaO and MgO lost to moles it is therefore possible to describe the $\omega - \psi$ plane in terms of maximum kg of CO_2 sequestered per kg protolith eroded (Figure S2a). This calculation assumes all weathering acidity is donated by carbonic acid and is therefore an upper-bound (Torres et al. 2014). We note that the period 0 – 0.5 Ga has a lower ω than other periods, likely reflecting an increase in biogenic carbonate contamination bias relative to other time periods (see 'Carbonate addition bias' section below).

Diagenetic Alteration

There is increasing evidence that diagenetic reactions between terrestrial sediments and pore-fluids are significant parts of the geochemical cycle of many elements (Sun et al. 2016). As the pH and geochemistry of porefluids evolves with depth, some primary minerals are dissolved, and reprecipitated as authigenic phases, changing the mineralogical composition of sediments as they are lithified. Three lines of evidence suggest our results have not been affected by this process. First, whilst these reactions affect mineralogy, so long as the reactions operate under closed-system conditions, use of bulk major-element data in aggregate is expected to be largely unaffected by this process. Given that the majority of siliciclastic sediments utilised in the SGP database are fine-grained and therefore low porosity, on this basis, closed-system diagenesis is expected (Bjørlykke and Jahren 2012). Assuming dominantly closed-system diagenesis, our results should therefore be insensitive to diagenetic reactions. There is further evidence to support this assertion. Second, we can test the influence of diagenesis on the major element record of marine fine grained sediments by comparing recent sedimentary rocks (0 – 0.5 Ga) to the major-element composition of the modern UCC as determined by surface sampling. This comparison shows that fine grained sediments produce a good match to the independently determined UCC composition. This suggests that diagenetic reactions have not biased the compositions of these recent sedimentary rocks. Finally, all of our principal findings are derived from aggregates of sediment geochemistry, either by generating composite samples (Table 1), or by calculating a smoothed trend of noisy data (Figure 3). Hence, any diagenetic transfer of material within the sedimentary column will likely be undone to some degree during our data analytical process.

We emphasise here that our model is unable to indicate where or when a particular compositional process may have acted. For example, open system chemical weathering which acts in the subsurface (e.g. anoxic marine silicate weathering; Wallmann et al. 2008) could have the same compositional effect as chemical weathering which acts in a sediment source region. By extension, recycling of ancient sedimentary rocks could also impart an inherited weathering signal into any subsequent sediments. The lack of a secular increase in weathering intensity over Earth's history suggests that this inheritance effect is not significant however.

Similarly, we have only explicitly considered cation exchange as acting on cations absorbed to clay particles. However, any

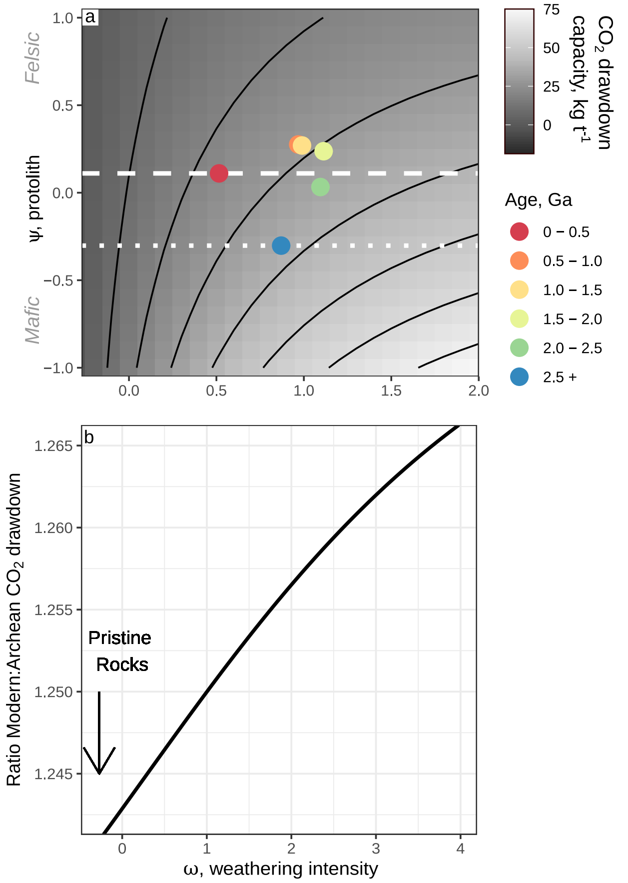

Supplementary Figure 2: **CO$_2$ drawdown capacity of sediments through time.** (a) ω-ψ plot overlain with contours of CO$_2$ drawdown capacity, calculated using the methods detailed in the main text. This is the amount of CO$_2$ that could be transferred from the atmosphere to the lithosphere via weathering, assuming all acidity is donated by carbonic acid. Value is given as kg of CO$_2$ removed from atmosphere per tonne rock eroded. Sediments with more mafic protoliths and greater weathering intensities result in higher potential CO$_2$ drawdown. Coloured points are the composite sediments from the indicated time periods. Dashed line corresponds to ψ value of period 0 - 0.5 Ga; Dotted line period 2.5 + Ga. The ω of the period 0 – 0.5 Ga is likely reduced relative to other time-periods due to carbonate contamination (see body text) (b) Ratio of Archean to present (0 - 0.5 Ga) CO$_2$ drawdown capacities for different ω values. Line is generated by dividing the CO$_2$ drawdown capacity along the dotted line by the values along the dashed line in Panel a. For the same weathering intensity, the Archean sedimentary protolith sequestered ~ 25 % more CO$_2$.

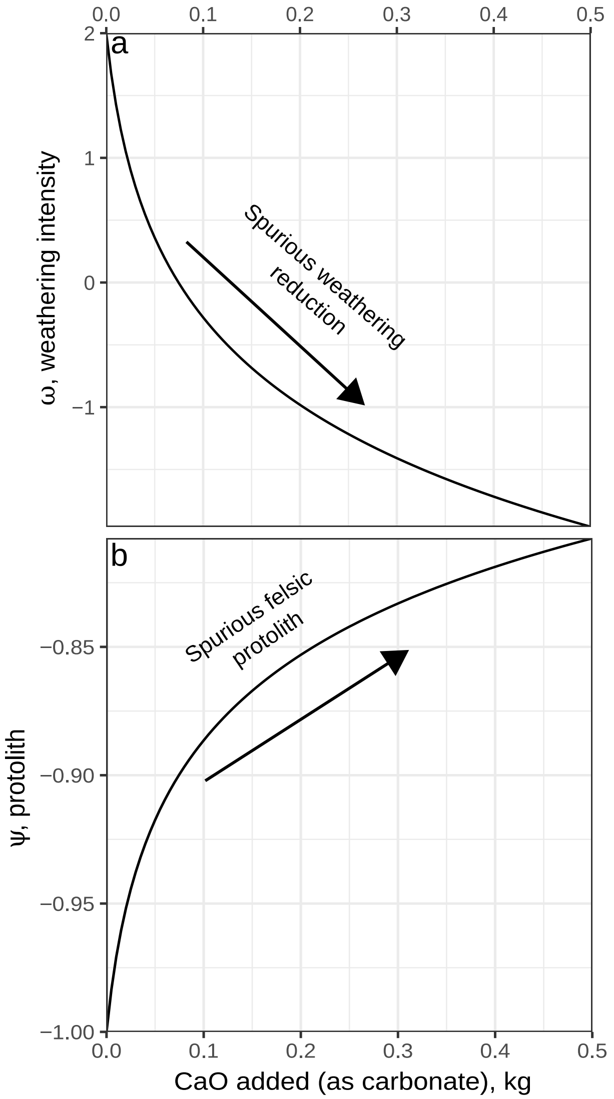

Supplementary Figure 3: **Exploring biases due to calcite addition** (a) Changes in ω coefficient resulting when increasing amounts of calcite are added to a composition with inital (ω, ψ) values of (2,-1). This suggests that the presence of any carbonate results in a spurious reduction in weathering intensity. (b) Changes in ψ coefficient resulting from same synthetic experiment as panel a. Calcite addition therefore introduces a spurious felsic bias. Note however that this bias is much smaller in magnitude than the bias introduced for ω.

reaction, diagenetic or otherwise, which is a net charge-balanced exchange of Ca for Na would produce the same compositional trend. This ambiguity is a limitation of any approach using purely elemental data.

Carbonate addition bias

Our model only explicitly considers the siliciclastic portion of a sediment. However, many sediments contain some portion of authigenic or biogenic carbonates, most commonly as calcite. As a result, it is important to understand the impact that calcite addition has on the interpretation of the ω and ψ coefficients. To investigate this effect we performed a synthetic experiment by increasing the amount of CaO in a sediment composition, and recalculated the ω and ψ coefficients. The results of this experiment are shown in Figure S3. Addition of calcite introduces a spurious reduction in weathering intensity. A spuriously more felsic protolith is also introduced, although the magnitude of this effect is much more minor. It is important to minimise the effect of these biases by screening samples from our dataset which are clearly affected by carbonate addition. Lacking mineralogical data it is generally challenging to identify carbonate contaminated samples. One approach is simply to remove samples which have CaO values above a certain cut-off value. However, given that cation exchange is another process which can increase the CaO this approach may be removing sediments which do not contain significant carbonate but simply have absorbed Ca. As a result, we identify the maximum amount of calcium which could be expected to be found in a sediment, if all of the sodium exchanges for calcium, for a standard range of protoliths. This corresponds to a sediment which derives from a basalt but has not undergone significant weathering. Hence, any sediment which has more calcium than this cut off value, if all the sodium is also exchanged, must also contain calcite and is thus excluded from consideration. This procedure is detailed more explicitly in the accompanying code (`github.com/AlexLipp/crustal-comp`).

Despite this filter, it is still likely that small amounts of calcite are present in many sediments from our dataset. As a result, our interpreted weathering intensities are likely an underestimate. To make sure that this bias is not the cause of the temporal trends in weathering intensity we see, we repeated our analysis with a more stringent carbonate filter (excluding all samples which had a positive CaO residual when cation exchange is not considered), but we observed similar trends. This suggests that whilst our data does likely incorporate the effect of carbonate addition, it does not affect the conclusions we have drawn.

Sampling Bias

The samples in our dataset are not homogenously distributed in time (Figure S1). As a result, for periods of low sample density, the average weathering trend we calculate will be more uncertain. To quantify this changing uncertainty interval we utilised a bootstrap resampling technique. Here, we resampled our dataset 1000 times with replacement. For each of these resampled datasets we generated a smoothed trend with the same 30 Myr Gaussian kernel. Then for each point in time we simply calculate the minimum and maximum possible values of the smoothed trend from these 1000 possible trends. These envelopes are shown as grey lines in Figure 3. This bounding envelope is wider in periods of lower sampling density reflecting the greater uncertainty of the average trend (Figure S1a).

An additional issue that can arise is if some particular stratigraphic units are 'oversampled' due to various reasons including accessibility of samples and particular economic interest. To investigate the robustness of our findings in the Phanerozoic against this issue we generate an analogous figure to Figure 3 but we instead take the mean ω value for individual stratigraphic units. We subsequently smooth these unit-averaged data points in the same way as before (i.e., applying a Gaussian filter of 30 Myr bandwidth and calculating the bootstrap uncertainties). The results of this analysis are displayed in Figure S4. The location of the the peaks and troughs in this trend are largely similar to the original trend in Figure 3. The trough in weathering intensity during the Ordovician/Silurian in Figure 3 is not however visible in this unit-averaged trend. It is notable that due to the smaller number of data points the bootstrap uncertainties are much higher than if samples are treated individually. This is particularly true for regions where only a small number of stratigraphic units have been sampled (Figure S1b).

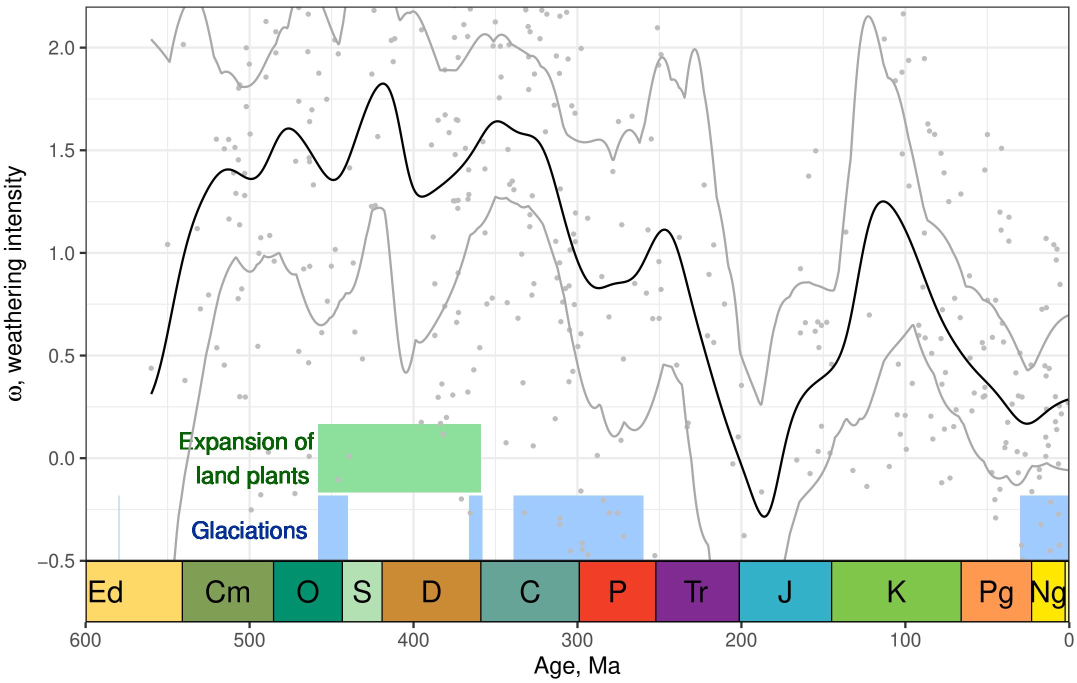

Supplementary Figure 4: **Weathering trend after averaging of ω values within stratigraphic units**. Grey points indicate average ω value of individual stratigraphic units. Black curve generated by smoothing data using 30 Myr Gaussian kernel. Grey lines indicate bounding envelope of 1000 bootstrap resamples of data. The general shape of this trend is similar to that displayed in Figure 3 although without a reduction in weathering intensity during the Ordovician/Silurian. Note the much greater uncertainty envelope than if all samples are treated individually.

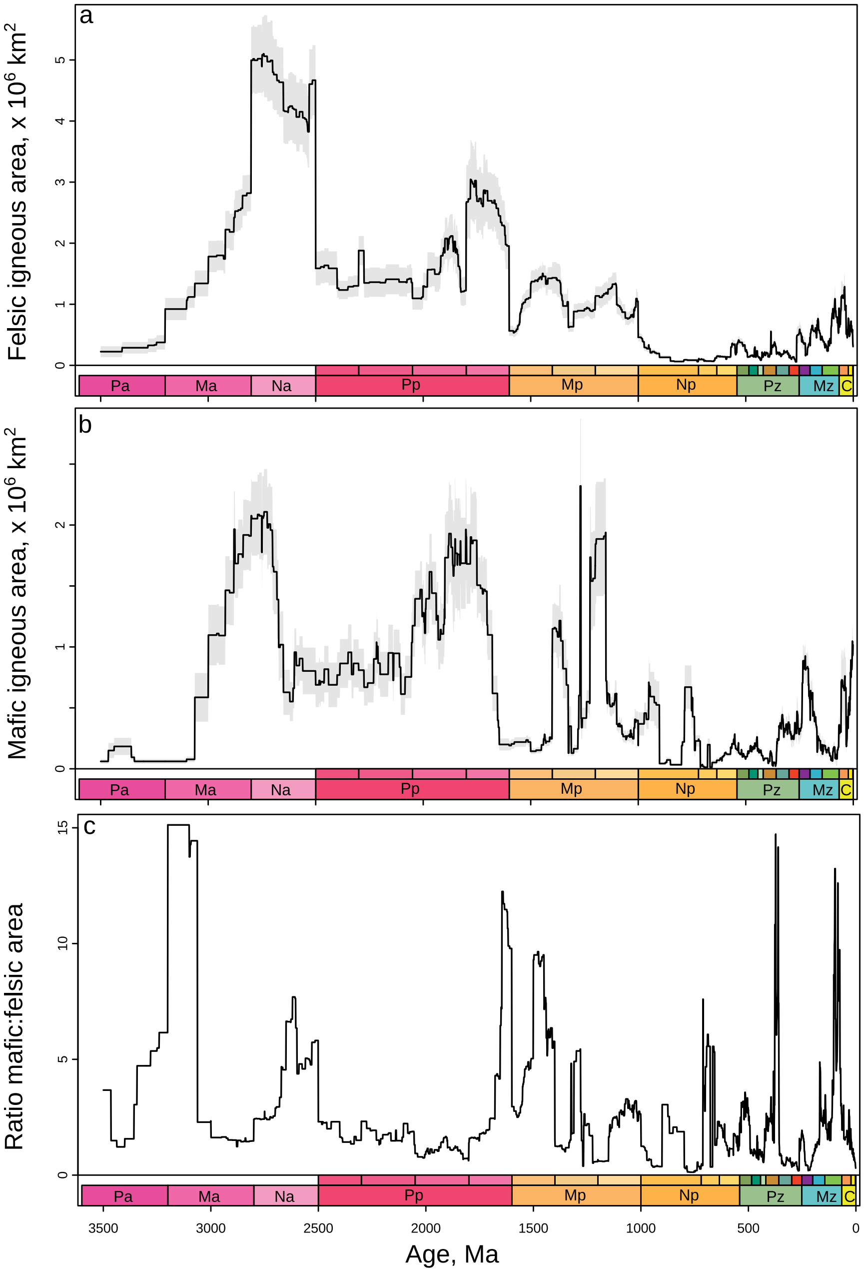

Supplementary Figure 5: **Areal extent of igneous rocks through time in Macrostrat database of geologic columns in North America (Peters et al. 2018)**. (a) Felsic area. (b) Mafic area. (c) Ratio of felsic to mafic area. Any secular trend in the mafic:felsic ratio is lower in magnitude than the short-term variability. This observation is consistent with the largely constant protolith diversity shown in Figure 2. Igneous rocks in the database are divided into 'felsic' and 'mafic' lithologies; all lithology classes can be found at `macrostrat.org/api/defs/lithologies?all`. Note that mafic and felsic rocks can co-occur in the same stratigraphic unit and are counted in both instances. Not all igneous rocks fall into one of these general lithology groups, and some names widely used in field descriptions (on which the Macrostrat classification is based, e.g., 'granite') are based on very broad compositional information. The Macrostrat API calls to extract data for this figure are found in the code repository.